Journal of Power Sources 260 (2014) 174–179

Contents lists available at ScienceDirect

Journal of Power Sources

journal homepage: www.elsevier.com/locate/jpowsour

Characterizations and electrochemical behaviors of milled Si with a degree of amorphization and its composite for Li-ion batteries

Byeong-Chul Yu [a], Yoon Hwa [a], Jae-Hun Kim [b], Hun-Joon Sohn [a,*]

[a] Department of Materials Science and Engineering, Seoul National University, Seoul 151-744, Republic of Korea
[b] School of Advanced Materials Engineering, Kookmin University, Seoul 136-702, Republic of Korea

HIGHLIGHTS

- Electrochemical behaviors of milled Si are characterized with a degree of amorphization.
- Unlike crystallite Si, partially amorphous Si starts to react with Li near 0.32 V.
- Graphite is coated onto the milled Si using a simple milling process.
- The m-Si/graphite composite with 0.11 V cut-off shows a good cycle performance with 800 mAh g^{-1} over 120 cycles.

GRAPHICAL ABSTRACT

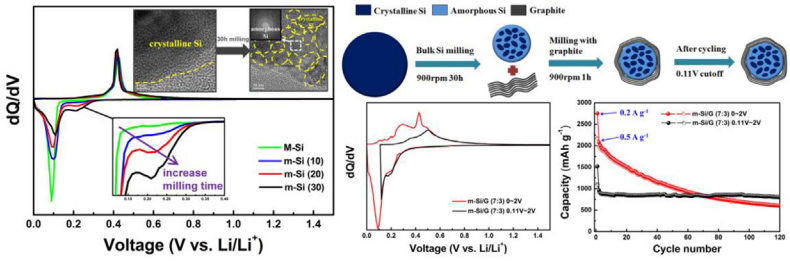

ARTICLE INFO

Article history:
Received 20 December 2013
Received in revised form
24 February 2014
Accepted 27 February 2014
Available online 12 March 2014

Keywords:
Amorphous silicon
High energy mechanical milling
Graphite
Anode

ABSTRACT

Electrochemical behaviors of milled Si using high energy mechanical milling (HEMM) process are characterized with a degree of amorphization. The amount of amorphous Si increases with milling time, and Si crystallites are embedded in the amorphous Si matrix. Unlike crystallite Si, partially amorphous Si starts to react with Li near 0.32 V. An intermediate LiSi phase is identified at 0.17 V during the first discharge of amorphous Si with Li. The milled Si/graphite (m-Si/G) composite prepared by using the simple HEMM process shows excellent electrochemical performance with a reversible capacity of 800 mAh g^{-1} at a rate of 0.5 A g^{-1} when cycled between 0.11 and 2.0 V.

1. Introduction

Rechargeable Li batteries with high energy capacity and long cycle life have received much attention for use in portable electronic devices, electric vehicles and implantable medical devices [1–4]. Si is an attractive anode material for Li secondary batteries because it has a low discharge potential and the highest known theoretical charge capacity (~4200 mAh g^{-1}) [5]. However, a large volume change (>300%) during Li alloying and dealloying can pulverize Si particles and electrically disconnect from the current collector [6]. To overcome these problems, several approaches have been suggested, including the preparation of nano active materials [6–11], active/inactive composite materials [12–14] and Si-based carbon composites [14–19]. These approaches have improved the electrochemical performance of Si-based anodes.

Among the Si based materials, amorphous Si (a-Si) shows better cycling performance than crystalline Si (c-Si) because the stress intensification due to anisotropic volume expansion of c-Si results in significantly increased tensile stress values along the <110> direction compared to the isotropic expansion of a-Si case [20–24].

* Corresponding author. Tel.: +82 2 880 7226; fax: +82 2 885 9671.
E-mail address: hjsohn@snu.ac.kr (H.-J. Sohn).

http://dx.doi.org/10.1016/j.jpowsour.2014.02.109
0378-7753/

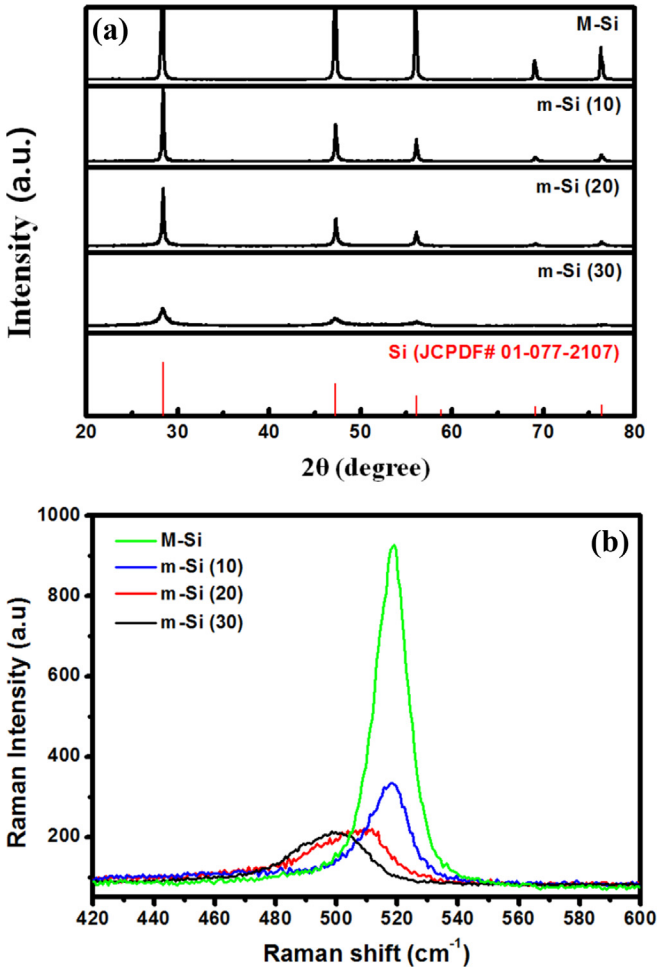

Fig. 1. (a) XRD patterns and (b) Raman spectra of M-Si, m-Si(10), m-Si(20) and m-Si(30) powders.

However, most of the methods for producing a-Si powder or film have relied upon a high cost synthesis process, namely chemical vapor deposition (CVD) [25–27]. a-Si can also be prepared by the high energy mechanical milling (HEMM) method, which decrease the particle size to produce a large amount of Si at one time [24,28]. Although Cui et al. showed that a-Si reacted with Li at a slightly higher potential than c-Si [29], electrochemical behaviors of a-Si using HEMM process have not been investigated fully. Such a comprehensive investigation would be important for designing Si based composites.

In this study, we investigate the degree of amorphization of milled Si for various milling times, and study the electrochemical behaviors of milled Si samples systematically. Based on the characteristics of milled Si, a milled-Si/graphite (m-Si/G) composite is prepared using simple HEMM, in which a few graphite layers are coated on the Si surface [30]. Since c-Si starts to react with Li below 0.11 V [31], the m-Si/G composite is tested as an anode between 2 and 0.11 V to investigate the electrochemical behavior of a-Si. Also previous studies have shown that the cycling life of a Si anode can be significantly improved by limiting the amount of Li that reacts with c-Si [29,32–34]. This approach, HEMM, would be attractive for practical applications because the starting materials and the synthetic processes are viable for large-scale production.

2. Experimental

2.1. Material preparation

Pure amorphous Si particles are not available commercially, and micron-size Si (M-Si) powder (Kosundo, 99%, 4 μm) was milled under Ar atmosphere using HEMM (Spex mill, 900 rpm) for various times (10, 20 and 30 h). Samples were referred to as m-Si (x), where (x) indicates the milling time. For the m-Si/G composite, m-Si (30) and graphite powders (MCMB, 10 μm) (7:3, by weight) were put into a 80 cm^3 hardened steel vial with stainless steel balls at a ball-to-powder ratio of 20:1. The HEMM process was conducted under Ar atmosphere for 1 h.

2.2. Materials characterization

All of the samples were examined using X-ray diffraction techniques (XRD, Rigaku, D-MAX2500) and Raman Spectrometer (HORIABA JobinYvon, T64000). A scanning electron microscope (SEM, JEOL, JSM-5600) was employed to observe the particle size of the milled Si samples, and high resolution transmission electron microscopy (HRTEM, JEOL, 3000F) analyses also were carried out to

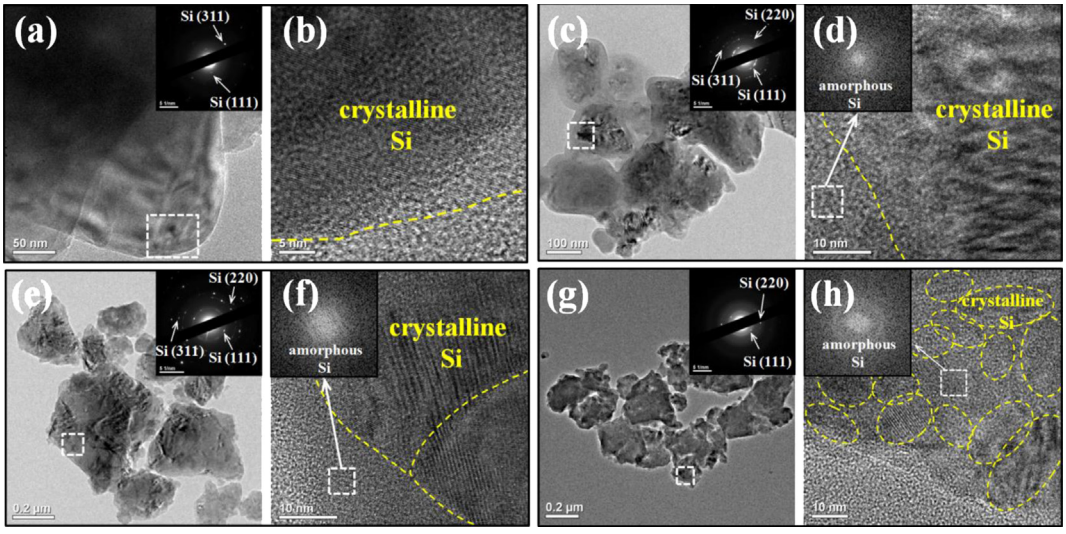

Fig. 2. Bright Field TEM image with SAED patterns and HRTEM images with FFT of (a,b): M-Si, (c,d): m-Si(10), (e,f): m-Si(20) and (g,h): m-Si (30).

confirm the microstructures of the milled Si samples and products during cycling. To prepare ex-situ TEM samples, electrodes were detached from the coin-type cell and washed with diethyl carbonate (DEC). Dilute suspensions of the samples were dropped onto a carbon-coated TEM grid. The ex situ HRTEM sample preparation processes were conducted in an Ar-filled glove box. Heat treatment of m-Si (30) sample was performed to identify the intermediate product of the Li–Si alloy phase at 0.17 V of the first discharge. A lithiated electrode was detached from the Cu foil, washed with DEC, placed into an alumina crucible, and sealed. The sample was heated at 500 °C for 12 h in Ar atmosphere. To confirm the graphite coating layer, the m-Si/G (7:3) sample was analyzed using TEM (Analytical TEM, JEOL, JEM-2100F) with EDS mapping.

2.3. Electrochemical cell test

The electrodes were prepared from a slurry composed of active material powders (70 wt.%), Super P (15 wt.%) as a conducting agent, and poly amide imide (PAI, 15 wt.%) as the binder. Slurry was made by mixing these components in a solvent N-methyl pyrrolidinone (NMP) at 60 °C and the slurry was coated onto copper foil. The samples were pressed and dried under vacuum at 200 °C for 4 h. A laboratory-made coin-type cell was used with Li foil as the counter and reference electrodes. The electrolyte contained 1 M $LiPF_6$and 10% fluoro ethylene carbonate (FEC) in ethylene carbonate (EC)/diethylenecarbonate (DEC) (3:7 vol.%, PANAX). All tests were performed galvanostatically using a Maccor automated tester in an Ar-filled glove box. Li was inserted into the working electrode during discharging, and extracted from the working electrode during charging.

3. Results and discussion

Fig. 1a shows the X-ray diffraction (XRD) patterns of the M-Si, m-Si (10), m-Si (20) and m-Si (30) samples. Although the M-Si sample (JCPDF# 01-077-2107) shows sharp Si peaks, the milled samples show low and gradually broadening peaks with milling time. The average crystallite size of the m-Si (30) sample is calculated to be approximately 16 nm from the Scherrer equation. To calculate the relative amounts of the crystalline and amorphous phases in the samples, the XRD results of each sample are deconvoluted, as shown in Fig. S1. According to the literature, the XRD pattern of a-Si shows two broad peaks centered at 2 theta values of about 29° and 52°, respectively. [35] The lines of the crystalline (blue line) and amorphous (red line) peaks are fitted to obtain the contribution of each peak. The amorphous volume fraction is calculated using the profile fit windows application (Philips analytical X-ray program) by the ratio of the area of amorphous to the whole area in XRD (black line). The amorphous volume fractions of M-Si, m-Si (10), m-Si (20) and m-Si (30) are 0%, 13%, 48% and 66%, respectively (Fig. S1a–d).

Fig. 1b displays the Raman spectra of the samples. The spectrum of the M-Si powder indicates a sharp peak at ~520 cm^{-1} corresponding to the crystalline Si phase. Although the peak intensity of the m-Si (10) powder deceases, the peak position does not change, indicating decreased grain size but predominantly constant crystalline Si phase. [36] The Raman peaks of the m-Si (20) and m-Si (30) shift towards a low frequency to 481 cm^{-1} due to partial amorphization of c-Si, in agreement with the other reports [28,37,38].

A scanning electron microscope (SEM) is conducted to confirm the particle size and elemental analyses (Fig. S2). Fig. S2a shows the M-Si powder, which has a few micron particles. And large particles still remain after the 10 h milling process (Fig. S2b). The particle size of the 20 h milling powder decreases to under 2 μm (Fig. S2c) and the m-Si (30) powder shows a similar size distribution (Fig. S2d).

Fig. 2 shows the bright field TEM and HRTEM images of the microstructure of each sample. The dark region of the M-Si powder indicates the crystalline Si phase (Fig. 2a), which is confirmed by the enlarged HRTEM image near the surface (Fig. 2b). The surface of the m-Si (10) particle is different from the core of the particle in the bright field TEM image (Fig. 2c). The crystalline Si is surrounded by the amorphous Si phase, as shown in the HRTEM with Fast Fourier transformed (FFT) images (Fig. 2d). A pressure of 7.9 GPa would be required for crystalline Si to undergo an amorphous phase transformation at room temperature [39]. The temperature during

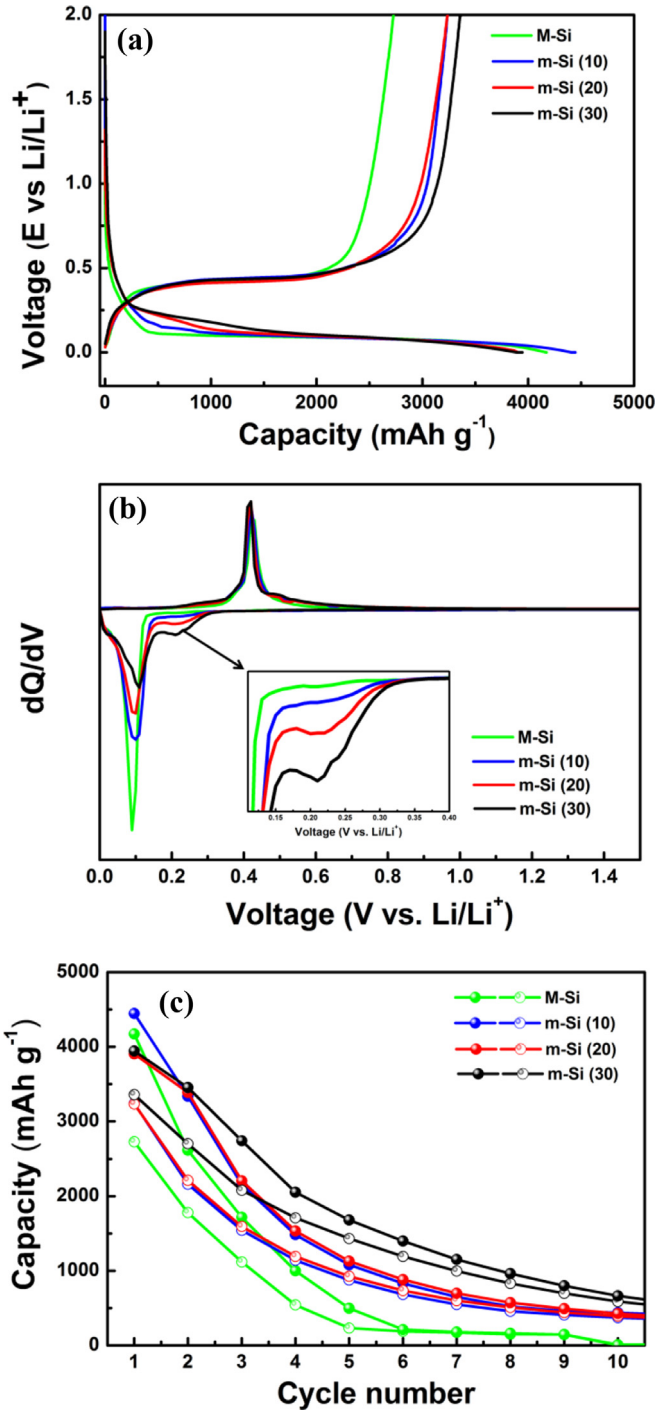

Fig. 3. Electrochemical tests at a current of 0.1 A g^{-1} (a) voltage profiles, (b) DCP (inset graph: magnified view of DCP of discharge from 0.4 V to 0.1 V)and (c) cycle performances of M-Si, m-Si(10), m-Si(20), and m-Si(30) powders.

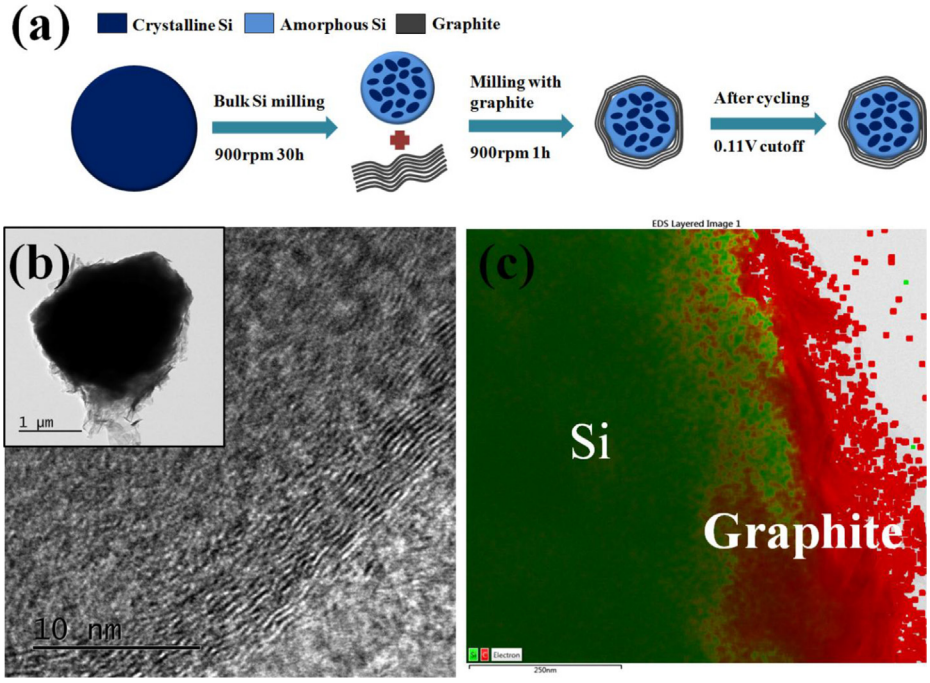

Fig. 4. (a) Schematic illustration of design process of the m-Si/G (7:3) composite, (b) HRTEM image (inset graph: Bright Filed TEM image) and (c) EDS mapping image of the m-Si/G (7:3) composite.

HEMM can rise to more than 200 °C and the pressure in the order of 6 GPa would be generated during HRMM [40]. Therefore, milling-induced amorphization is possible at particle surfaces because the pressure is infinitely high at the point contacts between particles [41]. For the m-Si (20) powder, the large dark regions still remain (Fig. 2e), and boundaries between c-Si grains are observed, indicating the decrease in the size of the Si crystallites (Fig. 2f). Unlike the above powders, the m-Si (30) powder shows a reduced dark region and dark spots within the particles after 30 h milling (Fig. 2g). c-Si (dotted region) of 10–20 nm size is distributed in the amorphous Si matrix, as shown in the HRTEM image (Fig. 2h). The crystallite size of m-Si (30) well agrees with the XRD data using the Scherrer equation in Fig. 1a. Also, the HRTEM and deconvoluted XRD results show that the degree of amorphization increases with milling time.

Each sample is tested as an anode material to investigate the effect of amorphization on the electrochemical behavior with milling time at a current of 0.1 A g^{-1} (Fig. 3). The voltage profiles are shown in Fig. 3a, and the first charge capacities of M-Si, m-Si (10), m-Si (20) and m-Si (30) are 2726, 3240, 3236, and 3358 mAh g^{-1}, with Coulombic efficiencies of 65%, 73%, 83%, and 85%, respectively. The first Coulombic efficiency of milled Si increases dramatically because of the improvement in the reversibility of Li with increasing amount of amorphous Si [24]. Fig. 3b shows the DCPs of the first cycle and difference in reaction behaviors during the discharge of milled Si and during the discharge of M-Si. As shown in the magnified DCP from 0.4 V to 0.1 V (inset graph in Fig. 2b), the M-Si starts to react with Li near 0.11 V and the flat region of voltage profile (0.1 V) corresponding to a sharp peak of DCP indicates transformation from a c-Si alloy to an a-Li_xSi alloy [42,43]. Unlike the M-Si sample, the milled Si reacts with Li at a higher voltage (~0.32 V). Furthermore, the reaction peak intensity of the milled Si at 0.22 V increases while that of c-Si at 0.1 V decreases gradually with milling time. These behaviors are related with the reaction of a-Si with Li at a higher voltage than the voltage at which the reaction of c-Si [29] takes place, this reaction at a higher voltage

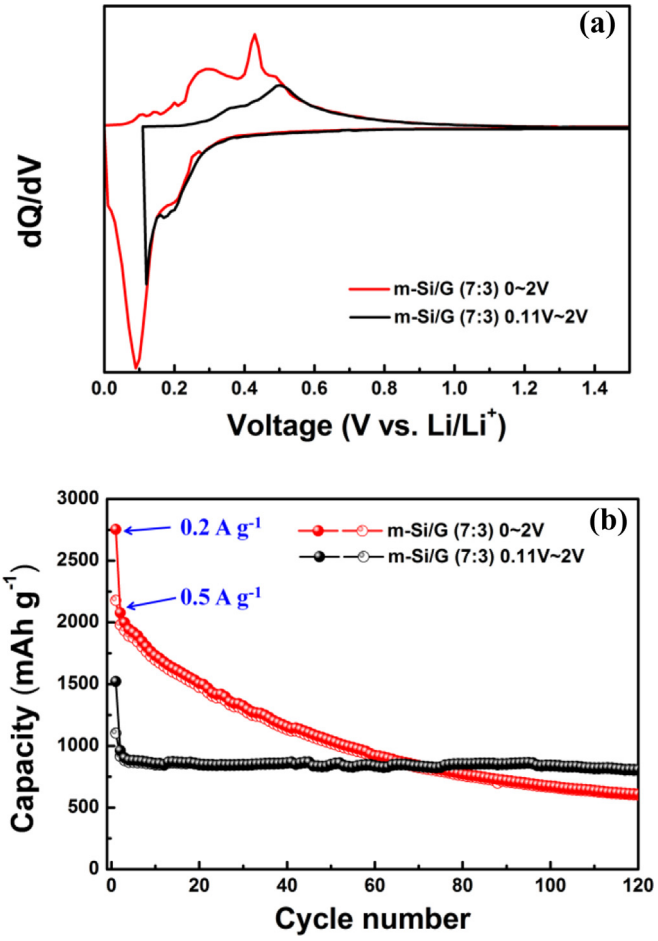

Fig. 5. Electrochemical tests (a) DCP of m-Si/G (7:3) and m-Si/G (7:3) with 0.11 V cut-off and (b) cycle performances (0.2 A g^{-1} for first cycle, 0.5 A g^{-1} for later cycles) of m-Si/G (7:3) and m-Si/G (7:3) samples with 0.11 V cut-off.

occurs because the energy to break up the Si–Si bond in the (111) plane is not required for a-Si [44]. To confirm the product of m-Si (30) at 0.17 V (first hump during discharge), ex-situ TEM is performed after heat treatment 500 °C for 12 h under Ar atmosphere (Fig. S3). Bright field TEM and HRTEM images with FFT are shown in Fig. S3a and b, respectively. The product is identified as a LiSi phase resulting from reaction of a-Si with Li, although a-$Li_{2.5}Si$ at ~0.21 V is reported based on the one dimensional thickness expansion of a fully a-Si thin film electrode [45]. Also the discharge capacity is 1190 mAh g^{-1} at 0.17 V, which is close to that of the LiSi phase (933 mAh g^{-1}) considering the contribution from the conducting agent (Super P) and the solid electrolyte interphase (SEI) formation. Fig. 3c compares with cycle performances of all samples during 10 cycles. Although the large reversible capacities lead to large volume expansions showing fast cycle fading, the amorphous Si in the milled Si samples positively affects the electrochemical performance of milled Si.

Based on the characterizations and electrochemical behaviors of milled Si, m-Si/graphite (m-Si/G) composite is prepared with m-Si (30) by an additional HEMM process for 1 h, as mentioned in the experimental section and described in Fig. 4a. Also, to suppress the volume expansion, the capacity of m-Si/G is limited by the voltage cut-off method [29,32–34]. The cut-off voltage of 0.11 V is used to observe the electrochemical behavior of the a-Si electrode since real-time NMR data shows that c-Si reaction with Li starts below 0.11 V [31].

Fig. S4a shows the XRD patterns of the m-Si/G composites consisting of m-Si (30) and graphite (JCPDF# 00-008-0415) of 70 wt% and 30 wt%, respectively. In Fig. S4b, the Raman spectrum of m-Si/G displays two peaks at 1360 and 1580 cm^{-1} corresponding to the disordered carbon (D band) and the crystalline graphite (G band), respectively [46]. Lu et al. reported that a D band peak corresponding to natural graphite develops after the ball milling process [47]. Fig. 4b displays the bright field TEM (inset graph) and HRTEM images of the m-Si/G composite. A few graphene layers are coated on milled Si surface. An HRTEM with energy dispersive spectroscopy (EDS) mapping images of the m-Si/G composite (Fig. 4c) clearly shows the Si core (green region) and graphene layer (red region).

Electrochemical tests of m-Si/G (7:3) are conducted, and the DCP of m-Si/G (7:3) at 0.11 V cut-off during discharge is compared with the DCP of the same sample without voltage cut-off in Fig. 5a. The two peaks that appear during lithiation of m-Si/G (7:3) are related with a-Si and c-Si reacting with Li as mentioned in Fig. 3b. The discharge peak at ~0.1 V for graphite is not visible because it is overlapped by the c-Si peak. The small charge peaks at 0.11 V and 0.15 V are due to the graphite in the composite. The charge peaks above 0.2 V are characteristic peaks of delithiation from c-$Li_{15}Si_4$ and a-Li_xSi. [30]. For the case of m-Si/G (7:3) with the 0.11 V cut-off, the second peak is partially limited during discharge, and broad and large 0.5 V peaks during charge appears, which are related with the transformation of the amorphous Li_xSi phase (x would be slightly larger than 1) to amorphous Si. And the contribution from graphite could be ignored with the 0.11 V cut-off case. Cycle performances are compared in Fig. 5b. All tests are conducted at a rate of 0.2 A g^{-1} for the first cycle and 0.5 A g^{-1} for later cycles. The discharge capacities of m-Si/G (7:3) and m-Si/G (7:3) samples with the 0.11 V cut-off are 2754 mAh g^{-1} and 1520 mAh g^{-1} at initial Coulombic efficiencies of 79.1% and 72.5%, respectively. The m-Si/G (7:3) sample with the 0.11 V cut-off shows excellent cycle performance,

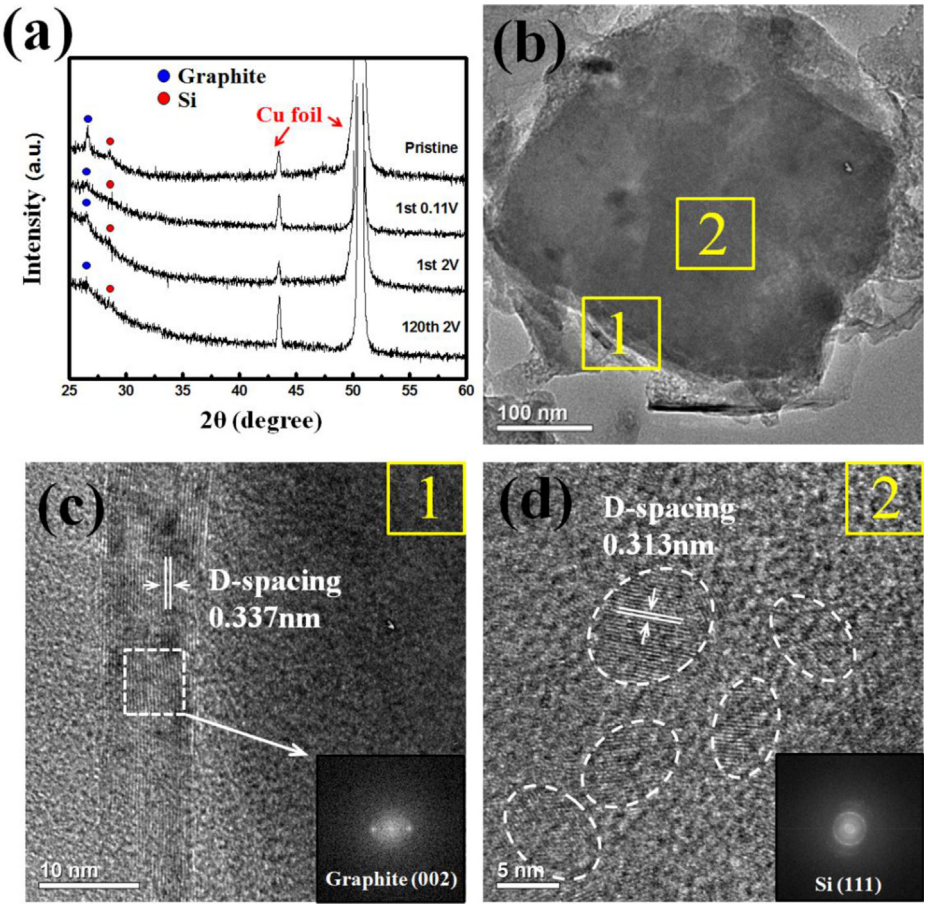

Fig. 6. Ex-situ analyses of m-Si/G with 0.11 V cut-off, (a) ex-situ XRD patterns of pristine electrode, 1st discharge at 0.11 V, 1st charge at 2 V and 120th charge at 2 V, ex-situ TEM (b) bright field image after 120th charge at 2 V, HRTEM images with FFT of (c) the surface (region 1) and (d) inside of particle (region 2).

that is reversible capacity of 801 mAh g^{-1} over 120 cycles, whereas the m-Si/G (7:3) sample exhibits fast cycle fading due to a large volume expansion. These results show that the voltage cut-off of m-Si/G (7:3) effectively prevents the reaction of c-Si with Li to improve the electrochemical performance of milled Si.

To further confirm the excellent electrochemical behavior of the m-Si/G sample with 0.11 V cut-off, ex-situ analyses by XRD and HRTEM are conducted after cycling, as shown in Fig. 6a. At 0.11 V of the first discharge, c-Si and graphite peaks remain, as expected, although peak intensities of the c-Si and graphite decrease. After charging at 2 V of the first and 120th cycle, the peaks of c-Si and graphite still remain, indicating that only a-Si reacts with Li during cycling. Fig. 6b shows the bright field TEM image charged at 2 V after 120 cycles. Liu et al. reported a critical particle diameter of ~150 nm, below which the particles neither cracked nor fractured upon lithiation [48]. In our sample, the structural integrity of particles after cycling is maintained without any cracks and fractures, even though the particle size is over ~300 nm since the volume expansion is less due to the voltage restriction during cycling (e.g. volume expansion due to the formation of the LiSi phase is only 33%). And the graphene layers with d-spacing of 0.337 nm are well attached on the surface of milled Si (region 1 in Fig. 6b) to provide a better electrical conduction path, as shown in Fig. 6c. Region 2 in Fig. 6b (inside of particle) shows that the nano c-Si does not react with Li and are distributed within the amorphous Si matrix (Fig. 6d), which agrees with ex-situ XRD data.

4. Conclusions

Milled Si with a degree of amorphization is characterized in this study. The amount of amorphous phase in bulk Si increases with milling time, and finally nano-crystalline Si embedded amorphous Si is obtain after 30 h of milling. The milled Si electrode shows the amorphous Si starts to react with Li at 0.32 V. The Li–Si product is LiSi alloy at 0.17 V. To utilize the milled Si, graphite is coated onto the milled Si using a simple milling process. The m-Si/G composite sample with 0.11 V cut-off shows better electrochemical performance, 800 mAh g^{-1} over 120 cycles at a rate of 0.5 A g^{-1}. This better performance is not only due to the electrical conductivity of the graphite on the surface but also due to the low volume expansion of the particles, which maintains the microstructural integrity of the particles without fracture during cycling.

Appendix A. Supplementary data

Supplementary data related to this article can be found at http://dx.doi.org/10.1016/j.jpowsour.2014.02.109.

References

[1] J.B. Goodenough, Y. Kim, Chem. Mater. 22 (2010) 587.
[2] M. Armand, J.M. Tarascon, Nature 451 (2008) 652.
[3] C.-M. Park, J.-H. Kim, H. Kim, H.-J. Sohn, Chem. Soc. Rev. 39 (2010) 3115.
[4] G. Jeong, Y.-U. Kim, H. Kim, Y.-J. Kim, H.-J. Sohn, Energy Environ. Sci. 4 (2011) 1986.
[5] B.A. Boukamp, G.C. Lesh, R.A. Huggins, J. Electrochem. Soc. 128 (1981) 723.
[6] U. Kasavajjula, C.S. Wang, A.J. Appleby, J. Power Sources 163 (2007) 1003.
[7] M. Green, E. Fielder, B. Scrosati, M. Wachtler, J.S. Moreno, Electrochem. Solid-State Lett. 6 (2003) A75.
[8] H. Li, X.J. Huang, L.Q. Chen, G.W. Zhou, Z. Zhang, D.P. Yu, Y.J. Mo, N. Pei, Solid-State Ionics 135 (2000) 181.
[9] X.W. Zhang, P.K. Patil, C.S. Wang, A.J. Appleby, F.E. Little, D.L. Cocke, J. Power Sources 125 (2004) 206.
[10] W.R. Liu, Z.Z. Guo, W.S. Young, D.T. Shieh, H.C. Wu, M.H. Yang, N.L. Wu, J. Power Sources 140 (2005) 139.
[11] T. Zhang, J. Gao, H.P. Zhang, L.C. Yang, Y.P. Wu, H.Q. Wu, Electrochem. Commun. 9 (2007) 886.
[12] O. Mao, R.L. Turner, I.A. Courtney, B.D. Fredericksen, M.I. Buckett, L.J. Krause, J.R. Dahn, Electrochem. Solid-State Lett. 2 (1999) 3.
[13] O. Mao, R.A. Dunlap, J.R. Dahn, J. Electrochem. Soc. 146 (1999) 405.
[14] I. Kim, P.N. Kumta, G.E. Blomgren, Electrochem. Solid-State Lett. 3 (2000) 493.
[15] I. Kim, P.N. Kumta, J. Power Sources 136 (2004) 145.
[16] M. Yoshio, S. Kugino, N.J. Dimov, J. Power Sources 153 (2006) 375.
[17] J. Yang, B.F. Wang, K. Wang, Y. Liu, J.Y. Xie, Z.S. Wen, Electrochem. Solid-State Lett. 6 (2003) A154.
[18] H.Y. Lee, S.M. Lee, J. Power Sources 112 (2002) 649.
[19] B.C. Kim, H. Uono, T. Satou, T. Fuse, T. Ishihara, M. Ue, M. Senna, J. Electrochem. Soc. 152 (2005) A523.
[20] J.T. Yin, M. Wada, K. Yamamoto, Y. Kitano, S. Tanase, T. Sakai, J. Electrochem. Soc. 153 (2006) A472.
[21] J.P. Maranchi, A.F. Hepp, P.N. Kumta, Electrochem. Solid-State Lett. 71 (2003) 1126.
[22] S. Ohara, J.J. Suzuki, K. Sekine, T. Takamura, Electrochemistry 71 (2003) 1126.
[23] L.Y. Beaulieu, K.W. Eberman, R.L. Turner, L.J. Krause, J.R. Dahn, Electrochem. Solid-State Lett. 4 (2001) A137.
[24] G.B. Cho, S.Y. Choi, J.P. Noh, Y.M. Jeon, K.T. Jung, T.H. Nam, J. Nanosci. Nanotechnol. 11 (2011) 6262.
[25] J.T. Harris, J.L. Hueso, B.A. Korgel, Chem. Mater. 22 (2010) 6378.
[26] L.E. Pell, A.D. Schricker, F.V. Mikulec, B.A. Korgel, Langmuir 20 (2004) 6546.
[27] S. Bourderau, T. Brousse, D.M. Schleich, J. Power Sources 81 (1999) 233.
[28] T.D. Shen, C.C. Koch, T.L. McCormick, R.J. Nemanich, J.Y. Huang, J.G. Huang, J. Mater. Res. 10 (1995) 1.
[29] L.-F. Cui, R. Ruffo, C.K. Chan, H. Peng, Y. Cui, Nano Lett. 9 (2009) 491.
[30] X. Chen, X. Li, F. Ding, W. Xu, J. Xiao, Y. Cao, P. Meduri, J. Liu, G.L. Graff, J.G. Zhang, Nano Lett. 12 (2012) 4124.
[31] B. Key, R. Bhattacharyya, M. Moecrette, V. Seznec, J.-M. Tarascon, C. Grey, J. Am. Chem. Soc. 131 (2009) 9239.
[32] M.N. Obrovac, L.J. Krause, J. Electrochem. Soc. 154 (2007) A103.
[33] W.R. Liu, M.H. Yang, H.C. Wu, S.M. Chiao, N.L. Wu, Electrochem. Solid-State Lett. 8 (2005) A100.
[34] L.F. Cui, Y. Yang, C.M. Hsu, Y. Cui, Nano Lett. 9 (2009) 3370.
[35] T.D. Hatchard, J.R. Dahn, J. Electrochem. Soc. 151 (2004) A1838.
[36] Z. Iqbal, S. Veprek, J. Phys. C 15 (1982) 377.
[37] J.E. Smith Jr., M.H. Brodsky, B.L. Crowder, M.I. Nathan, A. Pinczuk, Phys. Rev. Lett. 26 (1971) 642.
[38] R. Shuker, R.W. Gammon, Phys. Rev. Lett. 25 (1970) 222.
[39] M. Imai, T. Mitamura, K. Yaoita, K. Tsuji, High Press. Res. 15 (1996) 167.
[40] C. Suryanarayana, Prog. Mater. Sci. 46 (2001) 1.
[41] J.R. Groza, J. Mater. Eng. Perf. 2 (1993) 283.
[42] P. Limthingkul, Y.I. Jang, N.J. Dudney, Y.M. Chiang, Acta Mater. 51 (2003) 1104.
[43] C.K. Chan, H.L. Peng, G. Liu, K. Mcilwrath, X.F. Zhang, R.A. Huggins, Y. Cui, Nat. Nanotechnol. 3 (2008) 31.
[44] S.W. Lee, M.T. McDowell, J.W. Choi, Y. Cui, Nano Lett. 11 (2011) 3034.
[45] J.W. Wang, Y. He, F. Fan, X.H. Liu, S. Xia, Y. Liu, C.T. Harris, H. Li, J.Y. Huang, S.X. Mao, T. Zhu, Nano Lett. 13 (2013) 709.
[46] Y. Kawashima, G. Katagiri, Phys. Rev. B 52 (1995) 10053.
[47] M. Lu, Y. Tian, Y. Yang, Electrochim. Acta 54 (2009) 6792.
[48] X.H. Liu, L. Zhong, S. Huang, S.X. Mao, T. Zhu, J.Y. Huang, ACS Nano 6 (2012) 1522.